

Residual ANODE

Ranit Das,^{1,*} Gregor Kasieczka,^{2,†} and David Shih^{1,‡}

¹*NHETC, Dept. of Physics and Astronomy, Rutgers University, Piscataway, NJ 08854, USA*

²*Institut für Experimentalphysik, Universität Hamburg, 22761 Hamburg, Germany*

We present R-ANODE, a new method for data-driven, model-agnostic resonant anomaly detection that raises the bar for both performance and interpretability. The key to R-ANODE is to enhance the inductive bias of the anomaly detection task by fitting a normalizing flow directly to the small and unknown signal component, while holding fixed a background model (also a normalizing flow) learned from sidebands. In doing so, R-ANODE is able to outperform all classifier-based, weakly-supervised approaches, as well as the previous ANODE method which fit a density estimator to all of the data in the signal region instead of just the signal. We show that the method works equally well whether the unknown signal fraction is learned or fixed, and is even robust to signal fraction misspecification. Finally, with the learned signal model we can sample and gain qualitative insights into the underlying anomaly, which greatly enhances the interpretability of resonant anomaly detection and offers the possibility of simultaneously discovering and characterizing the new physics that could be hiding in the data.

I. INTRODUCTION

Despite countless searches at the LHC [1–7], so far none have turned up any definitive evidence for new physics beyond the Standard Model yet. Since the vast majority of these searches have been model-specific, there has been increasing interest [8–10] in developing new, model-agnostic search strategies powered by modern machine learning in recent years. The hope is that these will unlock vast, untapped discovery potential in the LHC data that has been missed by all the model-specific searches so far.

Among the model-agnostic search strategies proposed so far, methods for *resonant anomaly detection* – or using additional features x to enhance the sensitivity of a bump hunt in a primary resonant variable m – have received a lot of attention [11–31]. All of these methods have focused on learning good approximations to the Neyman-Pearson optimal anomaly detector:

$$R_{\text{optimal}}(x) = \frac{p_{\text{data}}(x)}{p_{\text{bg}}(x)} \quad (1)$$

Here x are the additional features, and $p_{\text{data}}(x)$ and $p_{\text{bg}}(x)$ are the data and background probability densities in the signal region (SR), defined as a window in m . Cutting on $R_{\text{optimal}}(x)$ can potentially enhance the significance of any anomaly in the signal region by a large amount.

The main strategy for learning R_{optimal} has been based on weak supervision: training a classifier between the data and a sample of events constructed to resemble the background as closely as possible. One exception to this has been ANODE [13], which is technically an *unsupervised* approach. With ANODE, one trains conditional

density estimators (normalizing flows in practice) on the signal region and sideband events, interpolates the latter into the SR, and constructs R_{optimal} by taking their ratio directly. Since this approach is solely based on unsupervised density estimation and does not involve any classifiers, it is technically an unsupervised approach to resonant anomaly detection.

It has been recognized [13, 17] that since density estimation is much more difficult than classification, ANODE suffers in sensitivity relative to classifier-based approaches. However, weak supervision and classifier-based approaches also have their drawbacks. In particular they do not perform well when the number of signal events is too small and they can be confused by noisy or uninformative features. Finally, the classifier by itself is not interpretable in that it does not tell us where the signal is, only where it is more overdense relative to the background.

In this paper, we remedy the sensitivity deficit of ANODE with a new twist on the method, which we will call *residual ANODE* or R-ANODE for short. The idea of R-ANODE is to explicitly fit to the signal component in the SR while holding the background fixed. Assuming data to be a mixture of the signal and background distributions

$$p_{\text{data}}(x, m) = w p_{\text{sig}}(x, m) + (1 - w) p_{\text{bg}}(x, m), \quad (2)$$

with w as the fraction of signal in the data, and $p_{\text{bg}}(x, m)$ as the fixed background template, we attempt to model $p_{\text{sig}}(x, m)$.

Fitting for the signal density directly, instead of the full data density, not only improves on the performance of ANODE, but it even surpasses the performance of the Idealized Anomaly Detector (IAD), which sets an upper bound to classifier-based approaches. The IAD was introduced in [17] and corresponds to training a classifier on data vs. perfectly simulated background (i.e. the same background model that the background in the data was drawn from). The IAD is limited by finite training statistics, noisy features and finite model capacity. So it

* ranit@physics.rutgers.edu

† gregor.kasieczka@uni-hamburg.de

‡ shih@physics.rutgers.edu

cannot fully approach the optimal anomaly detector or (by extension) the fully supervised classifier. R-ANODE is able to surpass the IAD since it assumes more about the signal vs. background mixture.

In R-ANODE, one has the option to fix the signal fraction w during training or to let it be a learnable parameter along with the signal density. We explore both options in this work, finding that for fixed w , the method is quite robust to w -misspecification, retaining excellent sensitivity to the signal even when w is larger or smaller than the true w by nearly an order of magnitude. For learnable w , we find that the method is robust and there is only a slight drop in overall signal sensitivity; furthermore, the learned w tracks the true w well down to a lower threshold of ~ 200 signal events. Thus R-ANODE could potentially be used to place measure or place limits on the signal fraction directly.

Finally, with the learned signal density, one can also draw potentially unbiased signal samples and directly learn about the properties of the new physics model hiding in the data. In this way, R-ANODE simultaneously offers significantly improved performance over other methods and also much greater interpretability.

This paper is organized as follows: Section II describes the R-ANODE method; Section III introduces the datasets and model definitions used in this work; Section IV describes our results, including training with fixed $w = w_{\text{true}}$ (Sec. IV A), scanning over fixed w (Sec. IV B), training with learnable w (Sec. IV C), and sampling from the learned signal model (Sec. IV D). Finally, Section V contains our conclusions and outlook. Appendix A describes further details of the architecture and hyperparameters used in our implementation of R-ANODE, and Appendix B contains more details about the learnable w case.

II. RESIDUAL ANODE METHOD

In R-ANODE we model the signal distribution $p_{\text{sig}}(x, m)$ for $m \in \text{SR}$ directly with a normalizing flow and use it to fit to data from equation (2). We minimize the negative log likelihood averaged over the SR data:

$$L = -\mathbb{E}_{x, m \sim \text{SR data}} \log p_{\text{data}}(x, m) \quad (3)$$

with respect to the parameters of $p_{\text{sig}}(x, m)$ while keeping $p_{\text{bg}}(x, m)$ fixed during training.

To obtain the joint background density in the SR from the sidebands, we break it up into two factors:

$$p_{\text{bg}}(x, m) = p_{\text{bg}}(x|m)p_{\text{bg}}(m) \quad (4)$$

The first factor, the conditional density $p_{\text{bg}}(x|m \in \text{SR})$, is obtained by interpolating from the sidebands similar to [13, 17]. The second factor, the background mass distribution $p_{\text{bg}}(m \in \text{SR})$, can be similarly obtained by interpolating from sidebands or (as we do in this work) approximating it with the data mass distribution under

the assumption that there is no statistically significant anomaly in the inclusive bump hunt. This allows us to get $p_{\text{bg}}(x, m)$ for $m \in \text{SR}$.

For the signal fraction w , we explore two options:

1. Hold w fixed during training. We then scan over different values of w , exploring the effect of fixing w to be larger or smaller than the true w .
2. Keep w as a learnable parameter during training, with the same optimizer and hyperparameters used for $p_{\text{sig}}(x, m)$.¹

We note that the true signal fraction w_{true} is related to the number of signal and background events in the SR:

$$w_{\text{true}} = \frac{N_{\text{sig, SR}}}{N_{\text{sig, SR}} + N_{\text{bg, SR}}} \quad (5)$$

For small amounts of signal that we assume throughout this work, this relation is approximately linear, i.e. $w_{\text{true}} \approx N_{\text{sig, SR}}/N_{\text{bg, SR}}$.

Finally, the anomaly score is constructed as

$$R(x, m) = \frac{p_{\text{sig}}(x, m)}{p_{\text{bg}}(x, m)}. \quad (6)$$

III. SETUP

A. Dataset

We use the LHCO R&D Dataset [8, 32] for our studies with dataset and train-val-test splits similar to [13, 17]. In the following, a brief summary of the dataset is given.

QCD dijet events form the Standard Model (SM) background, and $W' \rightarrow X(\rightarrow qq)Y(\rightarrow qq)$ events with $m_{W'} = 3.5 \text{ TeV}$, $m_X = 500 \text{ GeV}$ and $m_Y = 100 \text{ GeV}$ are used as signal. These are simulated using Pythia 8 [33, 34] and Delphes 3.4.1 [35–37]. The reconstructed particles are clustered into jets using the anti- k_T algorithm [38, 39] with $R = 1$ using Fastjet [40]. Events are required to satisfy the $p_T > 1.2 \text{ TeV}$ jet trigger.

The training features used are

$$m = m_{JJ}, \quad x = [m_{J_1}, \Delta m_J, \tau_{21}^{J_1}, \tau_{21}^{J_2}], \quad (7)$$

where invariant masses of the subjects satisfy $m_{J_1} < m_{J_2}$, and $\Delta m_J = m_{J_2} - m_{J_1}$. The n-subjettiness ratios are defined as $\tau_{ij} = \tau_i/\tau_j$ [41, 42].² The resonant variable is chosen as the dijet invariant mass m_{JJ} , with the signal

¹Using a different optimizer and hyperparameter to learn w might be interesting, but it could also necessitate further hyperparameter tuning, so we save this for future work.

²These features correspond to the baseline features defined in [29], along with the invariant mass m_{JJ} . We leave exploring the effects of noisy features, and extended set of features for a future study.

region (SR) defined as $m \in [3.3, 3.7]$ and its complement $m \notin [3.3, 3.7]$ forming the sideband (SB) regions.

For the primary dataset (meant to represent actual unlabeled data from the experiment), we use all 1-million SM background events from the original R&D dataset and inject different amounts of signal (1000 or lower) from the first 70k signal events of the R&D dataset. The amount of signal in the SR is approximately 76% of the total injected signal, i.e. $N_{\text{sig,SR}} \approx 0.76 \times N_{\text{sig}}$. Meanwhile, the amount of background in the SR is $N_{\text{bg,SR}} \approx 120,000$. The highest signal-injection of $N_{\text{sig}} = 1000$ corresponds to $\approx 2\sigma$ significance for the inclusive bump hunt in m_{JJ} (so, below discovery threshold).

All methods split this primary dataset into training and validation sets, with 80-20 split for R-ANODE, and 50-50 split for IAD and ANODE.³ For IAD, following [17], we used an additional 272k QCD dijet events in the SR [43] (with the same split as for data) to train the classifier. For evaluating SIC curves, we use the remaining 30k signal events from the original R&D dataset, along with the additional 340k QCD dijet events in the SR from [43].

For each N_{sig} , ten different datasets are produced by injecting different randomly selected signal events from the R&D dataset. These are used to derive error bars on the performance curves in the figures below.

B. Model architectures and selection

Here we briefly describe the model architectures and model selection procedures used in this work. More details can be found in Appendix A.

In [13, 17], the conditional normalizing flow models used to fit the data in the SR and SB regions were Masked Autoregressive Flows (MAF) with affine transformations [44, 45]. Here we use the same model for learning $p_{\text{bg}}(x|m)$ in the SB, but for learning $p_{\text{data}}(x|m)$ and $p_{\text{sig}}(x, m)$ in the SR (for ANODE and R-ANODE, respectively), we switch to RQS transformations [46] instead. Using the more expressive RQS transformations for the data and signal distributions was found to improve the performance of the methods. Interestingly, using RQS transformations for fitting the background in the SB led to *worse* results. Since RQS transformations are more expressive, it possibly leads to overfitting of the simpler background and/or interpolation.

For a proof of concept, $p_{\text{bg}}(m \in \text{SR})$ was estimated using the mass histograms of each full dataset using `scipy rv.histogram`. Even though the full data contains signal, this should be an excellent approximation to $p_{\text{bg}}(m)$ under our assumption that there is no significant excess in the inclusive bump hunt. In future work it would be

interesting to also compare this against a proper interpolation of the mass histogram from the sidebands.

Finally, for the IAD and fully supervised classifier, we utilize boosted decision trees (specifically a `HistGradientBoostingClassifier` from `scikit-learn` [47, 48]), which were shown in [29] to be robust under uninformative features.

For ANODE and R-ANODE, the method is trained on 20 random train/val splits of a given dataset, and for each split the 10 epochs with lowest validation losses are selected. Probabilities from these 200 models (or fewer in the case of learnable w , see Sec. IV C for details) are ensembled to obtain the final predictions of the methods. For the IAD, the model is retrained on 50 random train/val splits of a given dataset, and the models with lowest validation loss for each retraining are chosen to ensemble, similar to [29].

C. Performance metrics

The main performance metric we use in this paper is the Significance Improvement Characteristic (SIC). In terms of the signal efficiency (ϵ_S or TPR) and background efficiency (ϵ_B or FPR), one has

$$\text{SIC} = \frac{\epsilon_S}{\sqrt{\epsilon_B}} \quad (8)$$

The SIC characterizes the improvement to the nominal significance, using a cut on the anomaly score from a given method. We will also quote this nominal significance below, which is given by

$$\text{significance} = \text{SIC} \times \frac{N_{\text{sig,SR}}}{\sqrt{N_{\text{bg,SR}}}} \quad (9)$$

The latter factor is the nominal significance from the inclusive bump hunt (i.e. prior to any enhancement from a resonant anomaly detection method).

In general, the SIC depends on the working point, and we will exhibit this dependence by plotting SIC vs. the signal efficiency. At lower signal efficiencies, there are large statistical uncertainties in the SIC values. Hence we introduce a cut-off in the SIC curves when the relative statistical error on the background efficiency exceeds 20%.

It is also useful to quantify the performance at particular working points. Max SIC is defined as the maximum of all the SIC values above the cut-off for statistical stability. We also use SIC at FPR = 0.001 to represent a typical, fixed working point that an experiment might choose in practice.

IV. RESULTS

We first show the performance of an ideal version of R-ANODE with the correct value of $w = w_{\text{true}}$ fixed during

³Following previous work, we use the 50-50 split for ANODE and IAD. For R-ANODE, we found that the 80-20 split leads to a better performance as compared to the 50-50 split.

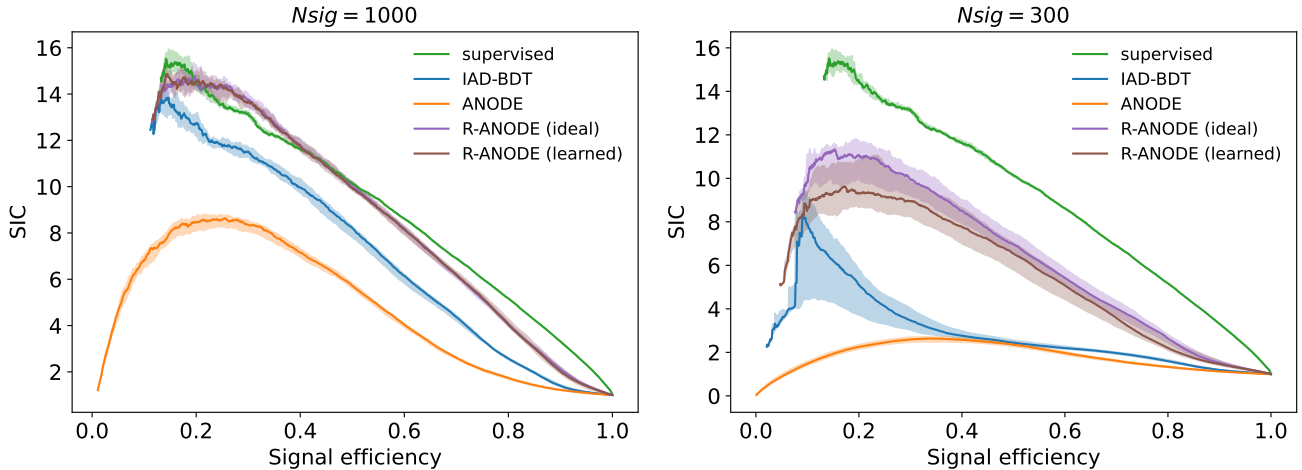


FIG. 1. SIC curves for $N_{\text{sig}} = 1000$ (left) and $N_{\text{sig}} = 300$ (right). R-ANODE with a learnable w almost saturates the performance of an idealized R-ANODE where w is fixed to its true value during training. Both these methods outperform the IAD and ANODE. The supervised classifier sets the upper limit for performance of all these methods, and at larger signal strengths, R-ANODE saturates this upper limit before the IAD does.

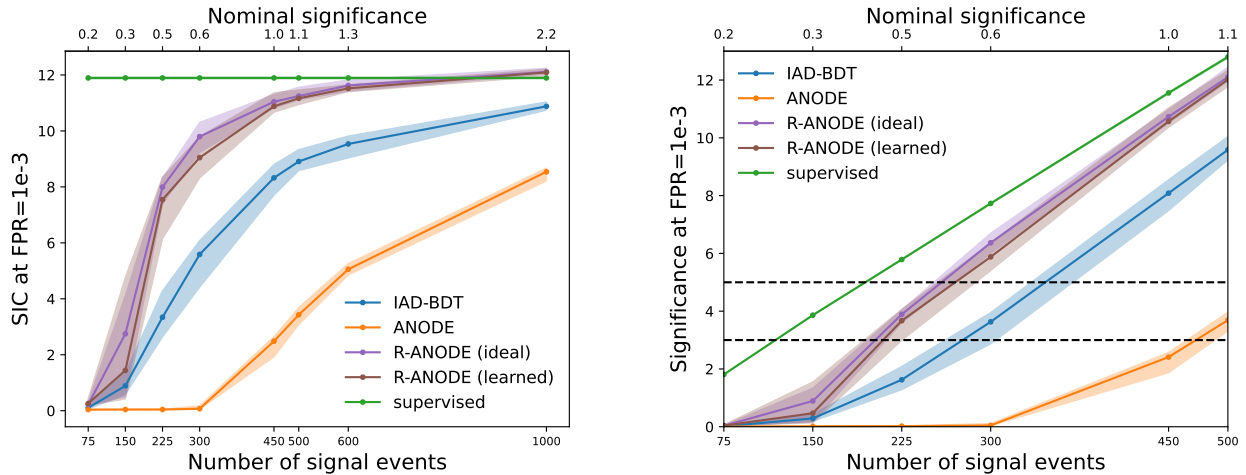


FIG. 2. Left: SIC (at FPR = 0.001) vs N_{sig} (amount of signal injected to data). Right: Total significance achieved (at FPR=0.001) vs N_{sig} . Again we see that R-ANODE with learnable w matches the idealized R-ANODE with $w = w_{\text{true}}$, and both outperform IAD and ANODE, across a wide range of signal levels.

training, for different amounts of injected signal. Then we present the results for different fixed values of w for $N_{\text{sig}} = 1000$. And finally, we show the results for the case where we attempt to learn w .

We compare R-ANODE to ANODE, the IAD, and a fully supervised classifier. For all figures, unless otherwise mentioned, the curves show the median value and 68% confidence bands for the results obtained by retraining the methods on 10 different datasets described in Sec. III A corresponding to different randomly-selected signal injections. Since the upper limit for performance of the classifier-based data-driven approaches like CWOLA [11, 12], CATHODE [17], CURTAINS [25], etc. is the IAD, we omit the explicit comparison to these methods. The supervised classifier sets the upper bound to per-

formance for all methods on this signal hypothesis. Interestingly, as observed in [17, 25, 29], for these signal injections there is a difference in performance between the IAD and supervised classifier. This is because the IAD is not actually fully optimal – it is limited by finite training statistics and finite model capacity. The truly optimal AD given by Eq. (1) would be completely equivalent to the fully supervised classifier, since it would be monotonic with it [17].

A. Idealized version: fixing $w = w_{\text{true}}$

We study the performance of R-ANODE for different amounts of signal-injections, in the idealized sce-

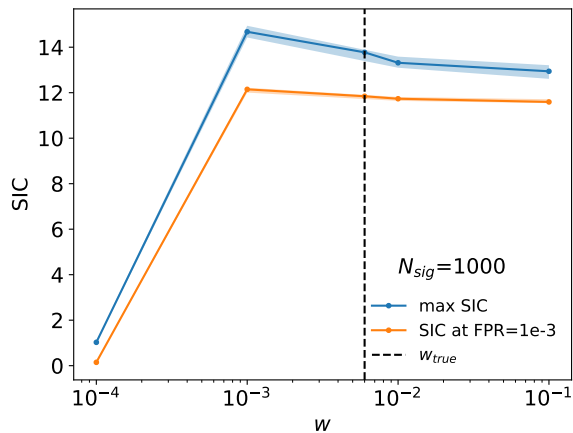


FIG. 3. For $N_{\text{sig}} = 1000$, we scan across different w -values, while holding it fixed during training. The significance improvement is robust for incorrect choices of w ; however the performance drops significantly for $w \ll w_{\text{true}}$.

nario where $w = w_{\text{true}}$ is held fixed during training. In Fig. 1, we show the SIC curves for $N_{\text{sig}} = 1000$ and $N_{\text{sig}} = 300$ (which correspond to 2.2σ and 0.7σ nominal inclusive significance in the SR, respectively). In both cases, the R-ANODE (ideal) method outperforms ANODE and the IAD across a wide range of signal efficiencies. For $N_{\text{sig}} = 1000$, R-ANODE (ideal) nearly closes the gap between the IAD and the fully supervised classifier⁴. Meanwhile, for $N_{\text{sig}} = 300$, we see that the gap between R-ANODE and the fully supervised classifier widens, but the gap with the IAD widens even further. The IAD suffers relative to the fully supervised classifier due to limited training statistics, whereas R-ANODE benefits from not being classifier-based and from its stronger inductive bias.

Next we examine the SIC values and total achieved significances at a fixed FPR of 10^{-3} . These are shown in Fig. 2 as a function of the number of injected signal events, for the different methods. We see from both plots that R-ANODE (ideal) achieves a better sensitivity to signal at all signal strengths, and allows us discover the signal at cross sections that are $\sim 25\%$ lower than the IAD.

B. Scanning fixed w

Next we study the more realistic case of scanning across different, fixed values of w during training. We

⁴Interestingly, R-ANODE even seems to outperform the fully supervised classifier for a small range of signal efficiencies. This shouldn't be possible and it may not be statistically significant, or it could point to a deficiency of the model architecture chosen for the fully supervised classifier.

focus on the benchmark case of $N_{\text{sig}} = 1000$ for simplicity.

From Fig. 3, we see that the performance curves and SIC values are actually quite robust to incorrect choices of w . We see that only at w -values an order of magnitude different than w_{true} is there some noticeable difference in the max SIC. At $w < w_{\text{true}}$, the trained signal model could be overestimating regions in phase space where the signal density is higher than background. This might help it locate the region with higher signal density easier, which could explain why in Fig. 3, we see a higher max SIC than w_{true} . At $w \ll w_{\text{true}}$, R-ANODE loses the capability of modeling the signal, which leads to a sharp decline in performance. This could be possibly used to put a lower bound on w . Finally, for $w > w_{\text{true}}$, the SIC declines slowly but does not completely go away. Here the method is learning to model the signal in addition to some amount of background. We expect as $w \rightarrow 1$, the R-ANODE method smoothly interpolates to the original ANODE method.

C. Learnable w

Finally, we explore what happens if we allow w to be learned during training. For simplicity, we use the same optimizer for w as the rest of the signal model, i.e. we just include w in the list of learnable parameters during training.

For each dataset – as described in Section III A – we take w -values from 20 retrainsings, and 10 lowest validation losses from each training. For learnable w , we find that some trainings converge to extremely low values of w . We label these trainings as having “undetected signal” and choose to exclude them from the analysis. To do so, we form histograms of the 200 learned w -values as shown in Fig. 6 of Appendix B. These histograms show a clearly well-separated, bi-modal structure, with one mode corresponding to the “undetected signal” case. We therefore devise a simple by-eye cut to remove this mode for a given dataset.

The remaining w -values are then averaged to produce a final output for the learned w for a given dataset. (The corresponding p_{sig} distributions are also averaged as described above, to produce the anomaly score, etc. in the learned w case.)

In Fig. 4, we show the final learned w vs. true w , for a range of N_{sig} values. We also indicate the spread of outcomes across the 10 different datasets as a blue uncertainty band. We see that for the most part, there is a good agreement between the learned w and true w values. At larger w there is a slight downward bias in the learned w , while at smaller w there is a pronounced upward bias. Indeed, for the no-signal fit, the learned w values have an average value of $\approx 10^{-3}$. According to Fig. 4, our method with learnable w is unable to detect $\lesssim 200$ signal events, for the given amount of background events.

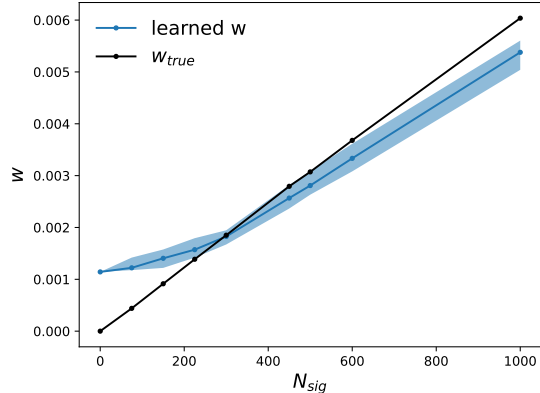


FIG. 4. A comparison between learned w and w_{true} for different N_{sig} values.

The undetectability of signal below some threshold may be an irreducible limitation of the R-ANODE method with learnable w , or it could be a by-product of our decision to exclude the “undetected signal” trainings and keep trainings where a nonzero w was returned. Ideally, one could devise a data-driven criterion that would correctly switch between the undetected and detected signal modes as N_{sig} decreases. Alternatively, one could stick to the current procedure and devise a process to quantify the lower threshold on signal strength in a data-driven way. For example, one could imagine applying R-ANODE to synthetic background events sampled from the interpolated sideband model $p_{\text{bg}}(x, m)$, which might enable us to measure the “floor” for w . We save such investigations for future work.

As noted in Section. IV B, R-ANODE as an anomaly detector is robust to incorrect choices of w . In Figs. 1 and 2, the R-ANODE performance curves with learnable w are shown in red. Although a slight performance drop relative to the idealized $w = w_{\text{true}}$ case is seen for lower signal strengths, overall it is encouraging to see that the performance of the learnable w case is actually extremely robust and nearly saturates the ideal R-ANODE performance.

D. Samples from the signal distribution

Using the IAD, one could make cuts on data with the anomaly score $R(x)$, to obtain the resulting signal samples. This requires a choice for the cut, which is not necessarily obvious from data. It also might leave too few signal events for interpretable distributions. Finally, the distributions one obtains would in general be biased, since the cut on $R(x)$ preferentially selects signal events that are more overdense relative to background. In R-ANODE however we benefit from being able to directly (over)sample signal events in an (in principle) unbiased

way.

In Fig. 5, we show a comparison of these signal densities obtained from R-ANODE (learned) for different signal-injections.⁵ We see that the learned signal densities show good qualitative agreement with the true signal densities and allow us to get rough estimates on properties of the signal, like the invariant mass, subjet-mass, pronginess of each subjet, etc. There is a clear degradation in the quality of the learned signal densities at lower signal strengths. Clearly, an important future direction here will be to devise data-driven methods to place uncertainties on these learned distributions.

V. CONCLUSIONS

R-ANODE is a novel method for model-agnostic, data-driven resonant anomaly detection that sets a new standard for the state-of-the-art in both performance and interpretability. The key to R-ANODE is to build in more inductive bias to the task of learning the optimal anomaly score. It builds on the previous approach of ANODE [13], but instead of fitting a density estimator for the data, it aims to isolate the small contribution from the unknown signal. By fitting a density estimator for just the signal component, holding fixed the background density learned from the sidebands, R-ANODE is able to better approach the optimal anomaly detector, surpassing approaches based on classifiers and weak supervision.

By learning the signal density, R-ANODE allows us to model the signal distributions directly from data, and this could be used to simultaneously discover and fully characterize the signal.

One of the issues we have not addressed in this paper and which we save for a future study is background estimation. Combining R-ANODE with a bump hunt would require us to examine the issue of mass sculpting in more detail, as was done in [21] for classifier-based approaches. Alternatively, perhaps the technique of “direct background estimation” from [13] could be revisited, or the uncertainties on the learned w could be properly calibrated somehow from data.

Another potential issue which we look forward to exploring further in future work is performance and robustness under the inclusion of additional, noisy high-level features [29, 30]. Perhaps the BDT-based density estimator used in [30] could be beneficial for this task, while speeding up the density estimation as well. Finally, it will be very interesting to go beyond high-level features and implement the R-ANODE method on the full phase space of jet constituents [31], where classifier-based approaches are especially challenged.

⁵We found that fixing to w_{true} didn’t improve these distributions much, hence we omit showing similar plots for R-ANODE (ideal).

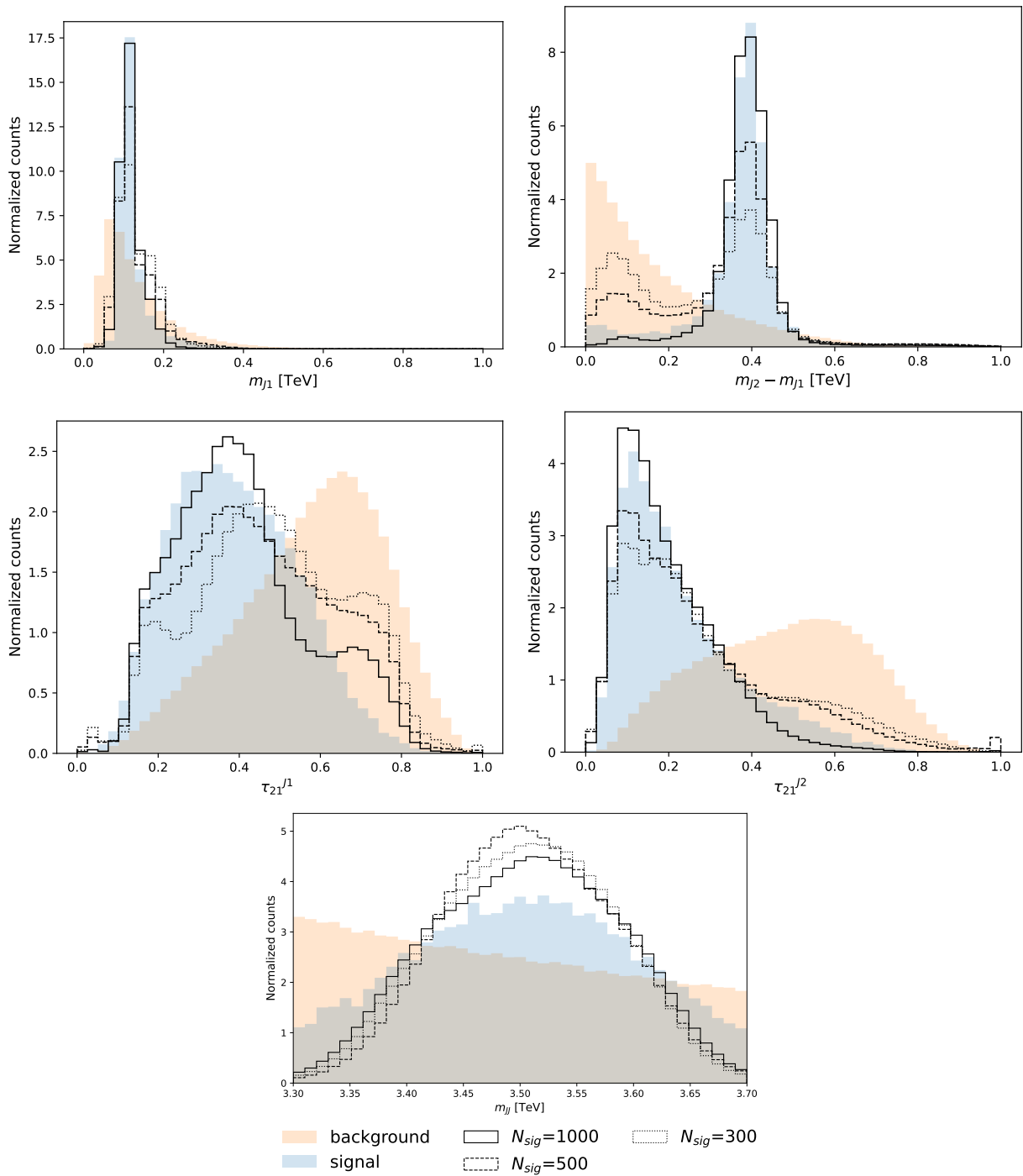


FIG. 5. Samples for R-ANODE with a learnable w during training, for $N_{sig} = [1000, 500, 300]$. Solid histograms show the true background (signal) distributions in orange (blue), while black lines indicate the signal distributions learned for different injected signal amounts. Overall, the qualitative agreement between the learned and actual signal distributions is decent, although the samples clearly get worse for lower signal injections due to insufficiency of training data.

ACKNOWLEDGEMENTS

We are grateful to Manuel Sommerhalder for assisting us with the scripts for training the background model in the SB. The work of RD and DS was supported

by DOE grant DE-SC0010008. GK acknowledges support by the Deutsche Forschungsgemeinschaft under Germany's Excellence Strategy – EXC 2121 Quantum Universe – 390833306. The authors acknowledge the Office of Advanced Research Computing (OARC) at Rutgers, The

State University of New Jersey <https://it.rutgers.edu/oarc> for providing access to the Amarel cluster and associated research computing resources that have contributed to the results reported here.

Appendix A: Implementation details

The background model $p_{\text{bg}}(x|m)$ is the same as [13, 17]: A Masked Autoregressive Flow(MAF) with affine transformations [44]. It contains 15 MADE blocks, with each block consisting of one hidden layer of 128 nodes. We train the density estimator using PyTorch [49] in the SB region for 100 epochs with Adam optimizer [50], with a learning rate of 10^{-4} , batch size 256, and batch normalization with a momentum of 1.0. The base distribution chosen is unit normal. The SB data is split into a training-validation split of 50-50, and models with 10 lowest validation losses are selected. The probabilities obtained from these 10 models are averaged to obtain $p_{\text{bg}}(x|m)$.⁶

For $p_{\text{sig}}(x, m)$ (fit to data in the SR only), we use RQS transformations [46] with 6 MADE blocks, with each block consisting of 2 hidden layers with 64 nodes, dropout 0.2, and batch-normalization is applied in between layers. The same model is also used for $p_{\text{data}}(x|m)$ in the SR for ANODE. The RQS-models for all cases are

trained with a unit normal base distribution, and a learning rate of 0.0003 with the AdamW [51] optimizer, with a batch size of 256 for 300 epochs. The train/val split and ensembling of p_{sig} and p_{data} were described in Sec. III B.

For the IAD and the fully supervised classifier, we train HistGradientBoostingClassifier with default hyperparameters for 200 epochs, similar to [29].

Similar to [17], the features x in the SB, are first shifted and scaled so that $x \in (0, 1)$, logit transformed, and then standardized with mean 0 and variance 1. The same pre-processing parameters from the SB, were reused for the SR, for all the methods. For R-ANODE and supervised, the mass is centered around zero, by subtracting 3.5 from all mass values.

Appendix B: Trainings with undetected signal

As mentioned in Section IV C, Fig. 6 shows the full histograms of learned w values, for different N_{sig} values (single dataset only). The “undetected signal” trainings where w converged to zero (up to machine precision) are clearly seen in the bi-modal histograms. The cuts shown in Fig. 6 are based on by-eye estimates, performed for each dataset, and all the results for R-ANODE (learned) are based on models corresponding to w -values surviving above these cuts.

-
- [1] ATLAS Collaboration, “Exotic Physics Searches,” (2023), <https://twiki.cern.ch/twiki/bin/view/AtlasPublic/ExoticsPublicResults>.
- [2] ATLAS Collaboration, “Supersymmetry searches,” (2023), <https://twiki.cern.ch/twiki/bin/view/AtlasPublic/SupersymmetryPublicResults>.
- [3] ATLAS Collaboration, “Higgs and Diboson Searches,” (2023), <https://twiki.cern.ch/twiki/bin/view/AtlasPublic/HDBSPublicResults>.
- [4] CMS Collaboration, “CMS Exotica Public Physics Results,” (2023), <https://twiki.cern.ch/twiki/bin/view/CMSPublic/PhysicsResultsEXO>.
- [5] CMS Collaboration, “CMS Supersymmetry Physics Results,” (2023), <https://twiki.cern.ch/twiki/bin/view/CMSPublic/PhysicsResultsSUS>.
- [6] CMS Collaboration, “CMS Beyond-two-generations (B2G) Public Physics Results,” (2023), <https://twiki.cern.ch/twiki/bin/view/CMSPublic/PhysicsResultsB2G>.
- [7] LHCb Collaboration, “Publications of the QCD, Electroweak and Exotica Working Group,” (2023), http://lhcbproject.web.cern.ch/lhcbproject/Publications/LHCbProjectPublic/Summary_QEE.html.
- [8] G. Kasieczka, B. Nachman, D. Shih, *et al.*, *Rept. Prog. Phys.* **84**, 124201 (2021), [arXiv:2101.08320 \[hep-ph\]](https://arxiv.org/abs/2101.08320).
- [9] T. Aarrestad *et al.*, (2021), [arXiv:2105.14027 \[hep-ph\]](https://arxiv.org/abs/2105.14027).
- [10] G. Karagiorgi, G. Kasieczka, S. Kravitz, B. Nachman, and D. Shih, *Nature Rev. Phys.* **4**, 399 (2022).
- [11] J. H. Collins, K. Howe, and B. Nachman, *Phys. Rev. Lett.* **121**, 241803 (2018), [arXiv:1805.02664 \[hep-ph\]](https://arxiv.org/abs/1805.02664).
- [12] J. H. Collins, K. Howe, and B. Nachman, *Phys. Rev. D* **99**, 014038 (2019), [arXiv:1902.02634 \[hep-ph\]](https://arxiv.org/abs/1902.02634).
- [13] B. Nachman and D. Shih, *Physical Review D* **101** (2020), [10.1103/physrevd.101.075042](https://doi.org/10.1103/physrevd.101.075042).
- [14] A. Andreassen, B. Nachman, and D. Shih, *Phys. Rev. D* **101**, 095004 (2020), [arXiv:2001.05001 \[hep-ph\]](https://arxiv.org/abs/2001.05001).
- [15] G. Stein, U. Seljak, and B. Dai, in *34th Conference on Neural Information Processing Systems* (2020) [arXiv:2012.11638 \[cs.LG\]](https://arxiv.org/abs/2012.11638).
- [16] O. Amram and C. M. Suarez, (2020), [10.1007/JHEP01\(2021\)153](https://arxiv.org/abs/2002.12376), [arXiv:2002.12376 \[hep-ph\]](https://arxiv.org/abs/2002.12376).
- [17] A. Hallin, J. Isaacson, G. Kasieczka, C. Krause, B. Nachman, T. Quadfasel, M. Schlaffer, D. Shih, and M. Sommerhalder, *Physical Review D* **106** (2022), [10.1103/physrevd.106.055006](https://doi.org/10.1103/physrevd.106.055006).
- [18] J. H. Collins, P. Martín-Ramiro, B. Nachman, and D. Shih, (2021), [arXiv:2104.02092 \[hep-ph\]](https://arxiv.org/abs/2104.02092).
- [19] K. Benkendorfer, L. L. Pottier, and B. Nachman, (2020), [arXiv:2009.02205 \[hep-ph\]](https://arxiv.org/abs/2009.02205).
- [20] G. Kasieczka, B. Nachman, and D. Shih (2021) [arXiv:2107.02821 \[stat.ML\]](https://arxiv.org/abs/2107.02821).
- [21] A. Hallin, G. Kasieczka, T. Quadfasel, D. Shih, and M. Sommerhalder, *Phys. Rev. D* **107**, 114012 (2023), [arXiv:2210.14924 \[hep-ph\]](https://arxiv.org/abs/2210.14924).

⁶For simplicity we use the same background model, obtained from a $N_{\text{sig}} = 1000$ case, as $p_{\text{bg}}(x|m)$ for all signal injections.

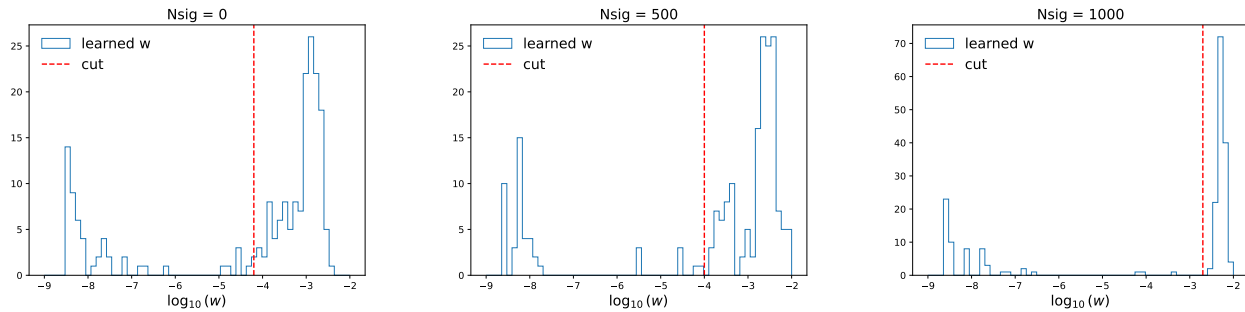


FIG. 6. Histograms of all 200 learned w values for three choices of N_{sig} (single dataset only). We see a clearly separated bimodal structure, with “undetected signal” trainings clustering at the low end (zero up to numerical precision). The red dashed lines are our thresholds for trainings with undetected signal; w values below these thresholds are rejected. The thresholds are decided dataset-by-dataset on the basis of a by-eye inspection.

- [22] M. F. Chen, B. Nachman, and F. Sala, *JHEP* **07**, 188 (2023), [arXiv:2212.10579 \[hep-ph\]](#).
- [23] J. F. Kamenik and M. Szewc, *Phys. Lett. B* **840**, 137836 (2023), [arXiv:2210.02226 \[hep-ph\]](#).
- [24] D. Sengupta, S. Klein, J. A. Raine, and T. Golling, (2023), [arXiv:2305.04646 \[hep-ph\]](#).
- [25] J. A. Raine, S. Klein, D. Sengupta, and T. Golling, *Front. Big Data* **6**, 899345 (2023), [arXiv:2203.09470 \[hep-ph\]](#).
- [26] T. Golling, G. Kasieczka, C. Krause, R. Mastandrea, B. Nachman, J. A. Raine, D. Sengupta, D. Shih, and M. Sommerhalder, (2023), [arXiv:2307.11157 \[hep-ph\]](#).
- [27] T. Golling, S. Klein, R. Mastandrea, and B. Nachman, *Physical Review D* **107** (2023), [10.1103/physrevd.107.096025](#).
- [28] G. Bickendorf, M. Drees, G. Kasieczka, C. Krause, and D. Shih, “Combining Resonant and Tail-based Anomaly Detection,” (2023), [arXiv:2309.12918 \[hep-ph\]](#).
- [29] T. Finke, M. Hein, G. Kasieczka, M. Krämer, A. Mück, P. Prangchaikul, T. Quadfasel, D. Shih, and M. Sommerhalder, “Back to the roots: Tree-based algorithms for weakly supervised anomaly detection,” (2023), [arXiv:2309.13111 \[hep-ph\]](#).
- [30] M. Freytsis, M. Perelstein, and Y. C. San, “Anomaly detection in presence of irrelevant features,” (2023), [arXiv:2310.13057 \[hep-ph\]](#).
- [31] E. Buhmann, C. Ewen, G. Kasieczka, V. Mikuni, B. Nachman, and D. Shih, “Full phase space resonant anomaly detection,” (2023), [arXiv:2310.06897 \[hep-ph\]](#).
- [32] G. Kasieczka, B. Nachman, and D. Shih, “R&D Dataset for LHC Olympics 2020 Anomaly Detection Challenge,” (2022).
- [33] T. Sjöstrand, S. Mrenna, and P. Skands, *Journal of High Energy Physics* **2006**, 026–026 (2006).
- [34] T. Sjöstrand, S. Mrenna, and P. Skands, *Computer Physics Communications* **178**, 852–867 (2008).
- [35] J. de Favereau, C. Delaere, P. Demin, A. Giammanco, V. Lemaître, A. Mertens, and M. Selvaggi, *Journal of High Energy Physics* **2014** (2014), [10.1007/jhep02\(2014\)057](#).
- [36] A. Mertens, *Journal of Physics: Conference Series* **608**, 012045 (2015).
- [37] M. Selvaggi, *Journal of Physics: Conference Series* **523**, 012033 (2014).
- [38] M. Cacciari and G. P. Salam, *Physics Letters B* **641**, 57–61 (2006).
- [39] M. Cacciari, G. P. Salam, and G. Soyez, *Journal of High Energy Physics* **2008**, 063–063 (2008).
- [40] M. Cacciari, G. P. Salam, and G. Soyez, *The European Physical Journal C* **72** (2012), [10.1140/epjc/s10052-012-1896-2](#).
- [41] J. Thaler and K. Van Tilburg, *Journal of High Energy Physics* **2011** (2011), [10.1007/jhep03\(2011\)015](#).
- [42] J. Thaler and K. Van Tilburg, *Journal of High Energy Physics* **2012** (2012), [10.1007/jhep02\(2012\)093](#).
- [43] D. Shih, “Additional QCD Background Events for LHC2020 R&D (signal region only),” (2021).
- [44] G. Papamakarios, T. Pavlakou, and I. Murray, “Masked autoregressive flow for density estimation,” (2018), [arXiv:1705.07057 \[stat.ML\]](#).
- [45] L. Dinh, D. Krueger, and Y. Bengio, “Nice: Non-linear independent components estimation,” (2015), [arXiv:1410.8516 \[cs.LG\]](#).
- [46] C. Durkan, A. Bekasov, I. Murray, and G. Papamakarios, “Neural spline flows,” (2019), [arXiv:1906.04032 \[stat.ML\]](#).
- [47] F. Pedregosa, G. Varoquaux, A. Gramfort, V. Michel, B. Thirion, O. Grisel, M. Blondel, P. Prettenhofer, R. Weiss, V. Dubourg, J. Vanderplas, A. Passos, D. Cournapeau, M. Brucher, M. Perrot, and Édouard Duchesnay, *Journal of Machine Learning Research* **12**, 2825 (2011).
- [48] G. Ke, Q. Meng, T. Finley, T. Wang, W. Chen, W. Ma, Q. Ye, and T.-Y. Liu, in *Advances in Neural Information Processing Systems*, Vol. 30, edited by I. Guyon, U. V. Luxburg, S. Bengio, H. Wallach, R. Fergus, S. Vishwanathan, and R. Garnett (Curran Associates, Inc., 2017).
- [49] A. Paszke, S. Gross, F. Massa, A. Lerer, J. Bradbury, G. Chanan, T. Killeen, Z. Lin, N. Gimelshein, L. Antiga, A. Desmaison, A. Köpf, E. Yang, Z. DeVito, M. Raison, A. Tejani, S. Chilamkurthy, B. Steiner, L. Fang, J. Bai, and S. Chintala, “Pytorch: An imperative style, high-performance deep learning library,” (2019), [arXiv:1912.01703 \[cs.LG\]](#).
- [50] D. P. Kingma and J. Ba, “Adam: A method for stochastic optimization,” (2017), [arXiv:1412.6980 \[cs.LG\]](#).
- [51] I. Loshchilov and F. Hutter, “Decoupled weight decay regularization,” (2019), [arXiv:1711.05101 \[cs.LG\]](#).